J Mater Sci (2006) 41:7597–7603
DOI 10.1007/s10853-006-0848-3

Formation of $LaFeO_3$ and thermal decomposition reactions in lanthanum(III) oxalate–iron(II) oxalate crystalline mixture

M. A. Gabal · S. S. Ata-Allah · A. O. Al-Youbi · S. N. Basahel · S. A. Al-Thabaiti

Received: 18 August 2005 / Accepted: 23 November 2005 / Published online: 11 October 2006

Abstract Thermal processes involved during the decomposition course of $La_2(C_2O_4)_3{\cdot}10H_2O$–$FeC_2O_4{\cdot}2H_2O$ (1:2 mole ratio) mixture up to 750 °C, in an atmosphere of air, were monitored by thermogravimetry and differential thermal analysis. X-ray diffraction and Mössbauer spectroscopy were used to characterize the intermediates and the final product. The results showed that a microcrystalline or possibly amorphous iron(III) oxide with a paramagnetic nature was appeared in the early stages of decomposition at 250 °C. By increasing the temperature, a well crystalline hematite with ferromagnetic properties was obtained. XRD pattern of the mixture calcined at 1100 °C shows the formation of $LaFeO_3$ single phase in consistent with the hyperfine magnetic splitting (one sextet of lines) characteristic of $LaFeO_3$ obtained in the Mössbauer spectra of the mixture calcined at the same temperature.

M. A. Gabal (✉)
Chemistry Department, Faculty of Science, Benha University, Benha, Egypt
e-mail: mgabalabdo@yahoo.com

S. S. Ata-Allah
Reactor and Neutron Physics Department, Nuclear Research Center, Atomic Energy Authority, Cairo, Egypt

A. O. Al-Youbi · S. N. Basahel · S. A. Al-Thabaiti
Chemistry Department, Faculty of Science, King Abdulaziz University, Jeddah, Saudi Arabia

Introduction

At high temperature the rare earth oxide, R_2O_3 (where R is yttrium or rare earth element) can react with iron(III) oxide to form orthoferrites; $RFeO_3$ with perovskite structure exhibiting weak ferromagnetism which have found important applications in modern telecommunications and electronic devices [1]. The Mössbauer spectroscopy, in combination with the other techniques has been used for the studying of the different properties of rare earth orthoferrites [2–4].

$LaFeO_3$ possesses very interesting properties, which make it particularly interesting for technological applications as a material for sensors. It has been proposed for the detection of humidity [5], alcohol [6], oxygen [7], CO [8] and NO [9]. The properties and the potential applications for which $LaFeO_3$ is used have generated a lot of research especially aimed at preparation and characterization. The properties of the final materials obtained are strongly dependent on the preparation method, as for most applications, the controlled synthesis of high purity $LaFeO_3$ powder is necessary for obtaining reproducible properties.

Although the conventional preparation method based on the solid-state reaction between La_2O_3 and Fe_2O_3 at high temperatures is a simple operation and uses inexpensive starting materials, it has some drawbacks such as secondary phase formation, crystal growth and limited degree of chemical homogeneity [10]. Development concerning new methods, especially solution techniques, namely thermal decomposition of wet chemically precipitated precursors, have been applied to lower the reaction temperature, improve synthesis conditions for obtaining pure phases and to prepare finer and homogeneous powder [11–14]. The

mechanochemical method can be also considered as an alternative route for the preparation [15].

The crystal structure refinement of XRD data of $LaFeO_3$ prepared either by the citrate amorphous precursor decomposition method at 900 °C [12] or by the thermal decomposition of the corresponding hexacyanocomplex at 1000 °C [16] showed that it crystallizes in the orthorhombic system. Vazquez et al. [17] prepared $LaFeO_3$ particles by sol–gel route, starting from a solution of corresponding metallic nitrates and using urea as a gelificant agent. Zhang and Saito have been synthesized LaFeO3 powder mechanochemically by room temperature grinding of La_2O_3 and Fe_2O_3 powders when the Fe_2O_3 sample with crystallite size less than 20 nm is used. With increase in the crystallite size Fe_2O_3 powder this solid reaction tends to be difficult.

Several studies [18, 19] and a review article [20] have been published concerning with the thermal decomposition of metal oxalates. Balboul et al. [18] investigated the thermal decomposition of $La_2(C_2O_4)_3{\cdot}10H_2O$ in air till 900 °C and characterized the intermediates and final solid product, La_2O_3 using XRD and IR-spectroscopy. The thermal decomposition of $FeC_2O_4{\cdot}2H_2O$ was investigated in air, oxygen and inert atmospheres using DTA–TG, Mössbauer spectroscopy and XRD techniques [19]. The final decomposition product in air was found to be Fe_2O_3, while in nitrogen, the residue obtained was found to be free iron, Fe_3O_4 and trace of FeO.

The main purpose of this paper is to characterize the thermal decomposition course of $La_2(C_2O_4)_3{\cdot}10H_2O$–$FeC_2O_4{\cdot}2H_2O$ (1:2 mole ratio) physical mixture to the onset of $LaFeO_3$ formation using DTA-TG, XRD and Mössbauer spectroscopy.

Experimental procedure

Materials

Pure metal oxalates, $La_2(C_2O_4)_3{\cdot}10H_2O$ and $FeC_2O_4{\cdot}2H_2O$ were synthesized by mixing aqueous solutions of stoichiometric amounts of analytical grade $LaCl_3{\cdot}7H_2O$ or $FeSO_4{\cdot}7H_2O$ with analytical pure reagent of oxalic acid under continuous stirring. The resulting precipitates were collected by suction filtration and then washed with water, ethanol before drying in a thermostated oven at about 50 °C.

The oxalate mixture $La_2(C_2O_4)_3{\cdot}10H_2O$–$FeC_2O_4{\cdot}2H_2O$ (1:2 mole ratio) was synthesized using the impregnation technique [21] in which few drops of bidistilled water was added to the desired mole ratios of the individual metal oxalates with vigorous stirring then the mixture was dried in a thermostated oven at 50 °C for 1 h.

Calcination products of the mixture were obtained by heating at various calcination temperatures chosen on the bases of the thermal analysis results. Thus samples of the mixture were thermally heated in an electrical oven for 30 min at 250, 600 or 750 °C; for 5 min at 430 °C or for 2 h at 900 or 1100 °C. The samples were then removed from the oven and cooled in air in a desiccator to room temperature. For simplicity, the calcination products are named in the text by LaFe followed by the calcination temperature (where LaFe refers to $La_2(C_2O_4)_3{\cdot}10H_2O$–$FeC_2O_4{\cdot}2H_2O$ (1:2 mole ratio) mixture). Thus LaFe-250 indicates decomposition product of LaFe at 250 °C.

Apparatus

Thermal analysis was performed using Shimadzu DT-40 (Japan). The thermogravimetry (TG) and differential thermal analysis (DTA) curves were recorded up to 1100 °C at heating rate of 5 °C min^{-1} in air atmosphere at flowing rate of 3 L h^{-1}. The weight of the sample in the Pt crucible was 10 mg. Highly sintered α-Al_2O_3 was the reference material for the DTA measurements.

X-ray powder diffraction (XRD) was carried out using a Philips PW 1710 diffractometer at ambient temperature. The instrument was used with a cobalt anode generating Fe-filtered Co–K_α radiation (λ = 1.7889 Å, 40 kV and 30 mA). Diffractograms were recorded in the 2θ range between 20 and 80°, with a divergence slit of 1°. For identification purpose, the relative intensities (I/I_0) and the d-spacing (Å) were compared with standard diffraction patterns of the ASTM powder diffraction files.

SEM is performed using Jeol T 300 (Japan) scanning electron microscope operated at 15 keV. Mixtures were mounted separately on aluminum substrates evacuated to 10^{-3} Torr and precoated (20 min, 5 min for each side of the four sides) in a sputter-coater with a thin uniform gold/palladium film to minimize charging in the electron beam. The applied voltage is 1.2–1.6 kV.

The Mössbauer spectra of the samples were recorded with a time mode spectrometer using a constant acceleration drive and a personal computer analyzer (PCA II-card with 1024 channel). The source is ^{57}Co in Rh matrix with an initial activity 50 mCi. Metallic iron spectra are used for the calibration of both observed velocities and hyperfine magnetic fields. The absorber thickness is approximately 10 mg cm^{-2} of

natural iron. Spectra were analyzed using the Mos-90 computer program [22].

Results and discussion

X-ray diffraction patterns of LaFe mixtures calcined at various temperatures are shown in Fig. 1. XRD pattern of the parent mixture at room temperature (Fig. 1a) gave the individual characteristic lines of both $La_2(C_2O_4)_3{\cdot}10H_2O$ (PDF No. 20-549) and $FeC_2O_4{\cdot}2H_2O$ (PDF No. 23-293).

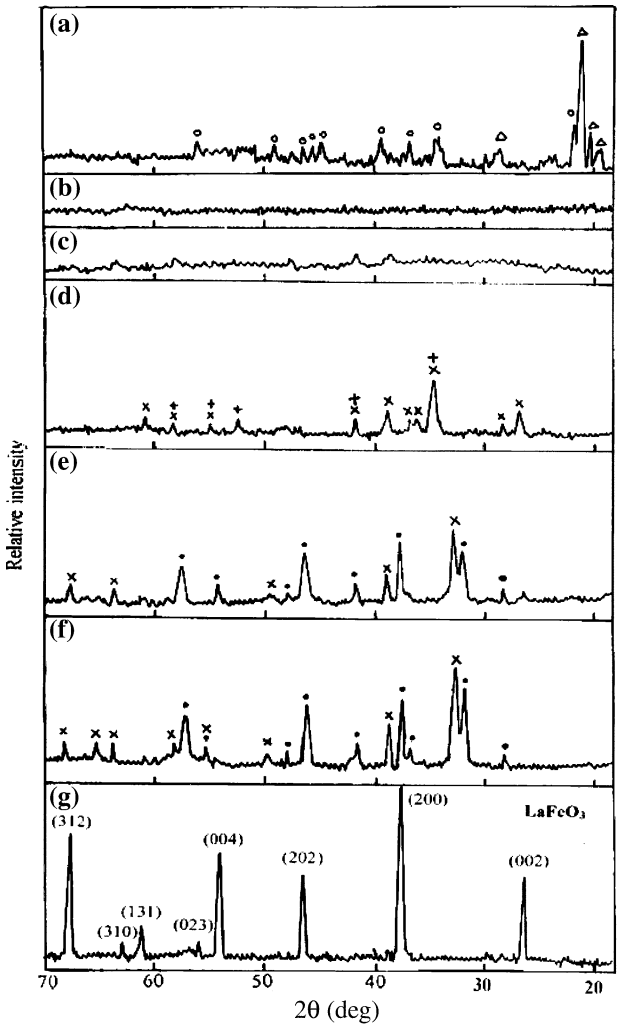

Fig. 1 Characteristic parts of XRD patterns of $La_2(C_2O_4)_3{\cdot}10H_2O$–$FeC_2O_4{\cdot}2H_2O$ (1:2 mole ratio) mixture calcined at different temperatures. (**a**) Parent mixture (**b**) Mixture calcined at 250 °C, (**c**) Mixture calcined at 425 °C, (**d**) Mixture calcined at 600 °C, (**e**) Mixture calcined at 750 °C, (**f**) Mixture calcined at 900 °C and (**g**) Mixture calcined at 1100 °C. Phases: (Δ)$La_2(C_2O_4)3{\cdot}10H_2O$, (o) $FeC_2O_4{\cdot}2H_2O$, (+) $La_2O_2CO_3$, (x) Fe_2O_3 and (•) La_2O_3

Mössbauer absorption spectra measured at room temperature for LaFe mixtures annealed at different temperatures are shown in Fig. 2. The Mössbauer

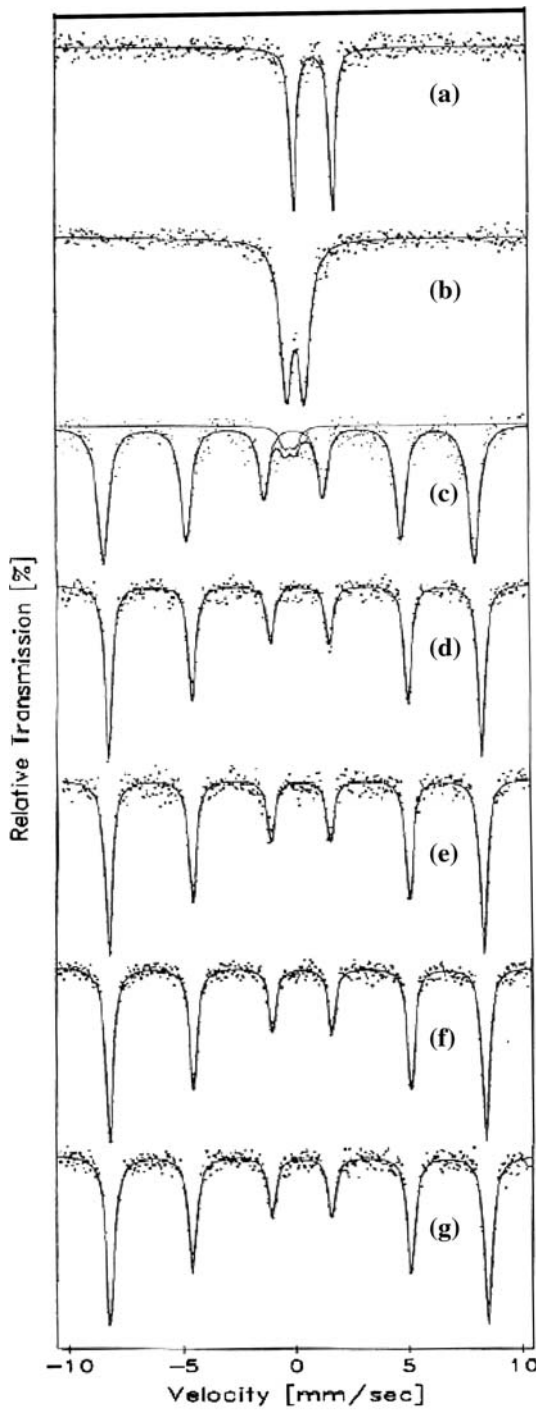

Fig. 2 The Mössbauer spectra of $La_2(C_2O_4)_3{\cdot}10H_2O$–$FeC_2O_4{\cdot}2H_2O$ (1:2 mole ratio) mixture calcined at different temperatures: (**a**) Parent mixture (**b**) Mixture calcined at 250 °C, (**c**) Mixture calcined at 425 °C, (**d**) Mixture calcined at 600 °C, (**e**) Mixture calcined at 750 °C, (**f**) Mixture calcined at 900 °C and (**g**) Mixture calcined at 1100 °C

spectrum of LaFe (Fig. 2a) reveals no magnetic interactions and shows a doublet with a large positive isomer shift (δ = 1.02 mm s^{-1}) and quadrupole splitting (ΔE_Q = 1.73 mm s^{-1}) as indication of divalent iron in $FeC_2O_4{\cdot}2H_2O$. The values associated with the dihydrate at room temperature are 1.02 and 1.7 mm s^{-1} for the isomer shift and the quadrupole splitting, respectively [23]. Also, the isomer shift value from the compilation by Fluck et al. [24] also for $FeC_2O_4{\cdot}2H_2O$ is 0.98 mm s^{-1}, which is close to the value observed in this paper.

TG and DTA curves obtained at heating rate of 5 °C min^{-1} (Fig. 1) show six weight loss (WL) processes (designated I–VI) in the decomposition course of LaFe mixture. Two of these processes (process, III, T_{max} = 214 °C and IV, T_{max} = 376 °C) are shown to be exothermic; whereas the others (process, I, T_{max} = 110 °C; II, T_{max} = 182 °C; V, T_{max} = 440 °C and VI, T_{max} = 660 °C) are endothermic.

The weight loss effected via the first two processes (I and II) accounts for the dehydration of $La_2(C_2O_4)_3{\cdot}10H_2O$ and $FeC_2O_4{\cdot}2H_2O$ in their mixture, respectively. The process I (WL = 16%) involves the elimination of 10 moles of water from hydrated lanthanum oxalate (theoretical WL = 16.6%), and process II (WL = 7%) leads to the removal of the four moles of hydration of two moles of ferrous oxalate (calculated WL = 6.7%), i.e. complete dehydration of the mixture with the formation of unhydrous oxalates mixture as follows:

$$La_2(C_2O_4)_3{\cdot}10H_2O{-}2FeC_2O_4{\cdot}2H_2O \xrightarrow{110^\circ C} La_2(C_2O_4)_3{-}2FeC_2O_4{\cdot}2H_2O \xrightarrow{182^\circ C} La_2(C_2O_4)_3{-}2FeC_2O_4$$

Water in crystalline hydrate may be considered as crystal water (eliminated at 150 °C and below), coordinated water (water eliminated at 200 °C and above) or co-coordinately linked as well as crystal water (eliminated at intermediate temperatures). This behaviors are attributed to different strength of the binding of these molecules in the crystal lattice which resulting in different dehydration temperatures [25]. Thus, the dehydration temperatures obtained in the present study suggests that, the water in hydrated lanthanum oxalate can be considered as crystal water whereas, that of the hydrated ferrous oxalate can be considered as coordinately linked as well as crystal water.

On further heating, process III follows immediately after the compilation of process II. The weight loss effected for this process, 35.5% is close to that expected, 35.1% which is attributed to the exothermic oxidative decomposition of ferrous oxalate in the mixture with the formation of $La_2(C_2O_4)_3$–Fe_2O_3 mixture as follows:

$$La_2(C_2O_4)_3 - 2FeC_2O_4{+}3O_2 \xrightarrow{214^\circ C} La_2(C_2O_4)_3 - Fe_2O_3{+}4CO_2$$

This decomposition route for ferrous oxalate was firstly suggested by Macklen [26] in which the decomposition of FeC_2O_4 is through two steps, the first was attributed to an increase in the valence of iron from Fe^{2+} to Fe^{3+} by the addition of oxygen and this is followed by rupture of the weakened Fe–O bond and the C–C bond to evolve CO_2 in the second step.

The completely amorphous X-ray diffraction pattern obtained for LaFe-250 mixture (Fig. 1b) suggests the formation of microcrystalline or possibly amorphous particles of ferric oxide.

In support of the above result, the Mössbauer spectrum of LaFe-250 mixture (Fig. 2b) shows a paramagnetic doublet, with an isomer shift (δ = 0.43 mm s^{-1}) and a positive quadrupole splitting (ΔE_Q = 0.79 mm s^{-1}), corresponding to the oxidation of iron(II) to a finely divided (or even possibly amorphous) iron(III) oxide. A similar paramagnetic component was appeared in the Mössbauer spectrum of finely divide iron(III) oxide prepared by the thermal decomposition of α–iron(III) oxide hydrate [27]. In our previous paper [28], the mixture of $CoC_2O_4{\cdot}2H_2O$–$FeC_2O_4{\cdot}2H_2O$ calcined at 245 °C produced a finely divided iron(III) oxide which is characterized by XRD, Mössbauer spectroscopy, FT–IR and SEM techniques.

$La_2(C_2O_4)_3$–Fe_2O_3 mixture is thermally stable up to 370 °C (Fig. 3), at which process IV (T_{max} = 376 °C) starts to operate. The total weight loss observed in this process at about 425 °C (ca. 44.5%) accounts for the formation of $La_2O(CO_3)_2$–Fe_2O_3 mixture (expected WL = 44.1%) as follows:

$$La_2(C_2O_4)_3 - Fe_2O_3 \xrightarrow{376^\circ C} La_2O(CO_3)_2 - Fe_2O_3 + CO_2 + 3CO$$

The exothermic nature of this decomposition process is attributed to the air oxidation of CO formed.

The XRD pattern of LaFe-425 °C (Fig. 1c) shows a large broadening of the diffraction peaks which suggests that the size of iron(III) oxide particles is still relatively small.

The Mössbauer spectrum of LaFe–425 mixture (Fig. 2c) consists of a six-line subspectra and a small absorption of a paramagnetic doublet. Thus it can be suggested that the mixture fired at 425 °C is of ferri-

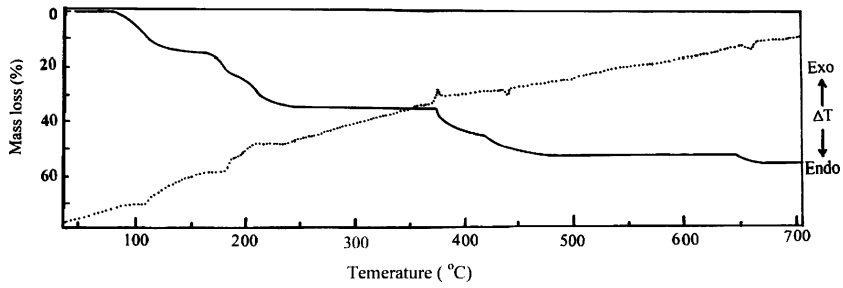

Fig. 3 DTA–TG curves of $La_2(C_2O_4)_3{\cdot}10H_2O$–$FeC_2O_4{\cdot}2H_2O$ (1:2 mole ratio) mixture in air at heating rate of 5°C min^{-1}

magnetic and paramagnetic nature, simultaneously. One part of the mixture has a volume too small to maintain the ferrimagnetic properties and the other has a size large enough to become ferrimagnetic. The broad size distribution is one reason why the mixture becomes paramagnetic and ferrimagnetic simultaneously. The ratio of the different magnetic phases is based on the calculated absorption ratio of the two subspectra. The doublet subspectra has a very small absorption ratio (6%) compared with that of the ferrimagnetic one. The values of isomer shift and the quadrupole splitting associated with the paramagnetic subspectra are 0.40 and 0.45 mm s^{-1}, respectively. The ferrimagnetic subspectra shows an isomer shift of 0.44 mm s^{-1} and a negative quadrupole splitting of –0.20 mm s^{-1}. The obtained hyperfine magnetic splitting (497 kOe) is significantly less than the normal value of iron(III) oxide, with larger particle size, of 515 kOe [29]. The XRD pattern and the Mössbauer spectrum of $CdC_2O_4{\cdot}3H_2O$–$FeC_2O_4{\cdot}2H_2O$ (1:2 mole ratio) mixture [21] calcined at 400 °C showed a similar behavior to that obtained in this work. The absorption ratio of the paramagnetic subspectra was observed to decrease relative to that in LaFe-250 mixture which suggests the successive crystallization of Fe_2O_3 with increasing the calcination temperature.

Upon further heating, process IV overlapped by a rapid endothermic weight loss process (process V; T_{max} = 440 °C). This brings the total WL up to 54% at about 600 °C, which is close to the 53.5% calculated for the formation of $La_2O_2CO_3$–Fe_2O_3 mixture as follows:

$$La_2O(CO_3)_2 - Fe_2O_3 \xrightarrow{440^\circ C} La_2O_2CO_3 - Fe_2O_3 + CO_2$$

The XRD pattern of LaFe–600 (Fig. 1d) shows the characteristic XRD lines of $La_2O_2CO_3$ (PDF No. 25-424) and Fe_2O_3 (PDF No. 13-534).

The Mössbauer spectrum of LaFe-600 mixture (Fig. 2d) reveals the disappearance of the paramagnetic component of Fe_2O_3 and displays only the ferrimagnetic Fe_2O_3 component with larger particle size. The six line pattern obtained shows an isomer shift (δ = 0.44 mm s^{-1}), a more negative quadrupole splitting (ΔE_Q = –0.22 mm s^{-1}) relative to that obtained for LaFe–425 mixture and magnetic hyperfine splitting (513 kOe) which is nearly equal to that of the normal magnetically oriented Fe_2O_3 [29].

As the temperature goes up (Fig. 3), process VI takes place endothermically (T_{max} = 660 °C). This process brings the total WL to 57%, which is close to that expected (56.2%) for the overall conversion of LaFe mixture to La_2O_3–Fe_2O_3 mixture as follows:

$$La_2O_2CO_3 - Fe_2O_3 \xrightarrow{660^\circ C} La_2O_3 - Fe_2O_3 + CO_2$$

From the above thermal analysis results it is clear that, the thermal decomposition behavior of the metal oxalates in their mixture resemble with those of the individual metal oxalates [18, 26] which suggests the absence of any chemical reactions between the two metal oxalate s in their mixture since each one behave as it is present alone.

XRD of LaFe–750 mixture (Fig. 1e) exhibits the presence of the characteristic lines of La_2O_3 (PDF No. 22-641) And Fe_2O_3 (PDF No. 13-534). At the same time, no characteristic lines of $LaFeO_3$ were appeared. This suggests the absence of any reaction between La_2O_3 and Fe_2O_3 at this temperature range.

Moreover, the Mössbauer spectrum of LaFe-750 mixture shows a similar magnetic splitting pattern as those obtained for LaFe-600 with nearly the same magnetic parameters.

By increasing the calcination temperature to 900 °C, both the XRD pattern (Fig. 1f) and the Mössbauer spectrum (Fig. 2f) give the same behavior as those obtained for LaFe-750, which suggests again the inability of the orthoferrites formation up to this temperature.

The intensifying of the XRD peaks characteristic of Fe_2O_3 with rising temperature from 425 °C up to 900 °C suggests the improving in the crystallinity of the oxide formed. Moreover, the decrease of the peak width in LaFe-900 (Fig. 1f) signifies sintering of material particles.

According to the X-ray diffraction pattern obtained for LaFe-1100 mixture (Fig. 1g), the disappearance of any XRD lines characteristic of La_2O_3 or Fe_2O_3 with the appearance of the intensive XRD lines characteristic for $LaFeO_3$ (PDF No. 15-148) indicates the complete formation of the orthoferrite at this temperature. The calculated lattice parameters; a = 5.5667 Å, b = 7.8401 Å and c = 5.5969 Å are in close agreement with those reported by Falcon et al. [12] For LaFeO3 synthesized at 900°C by the citrate amorphous precursor decomposition method (a = 5.5647 Å, b = 7.8551 Å and c = 5.5560 Å).

It is well known that [30] the ^{57}Fe Mössbauer spectra of the rare earth orthoferrites, $RFeO_3$ (where R = rare earth element), shows hyperfine magnetic splitting (one sextet of lines). Thus the six lines pattern obtained in the Mössbauer spectrum of LaFe–1100 mixture (Fig. 2g) can be ascribed to the formation of $LaFeO_3$ in support to the XRD results. The isomer shift and the hyperfine magnetic splitting from the compilation by Jiangong et al. [31] for $LaFeO_3$ are 0.41 mm s^{-1} and 520 kOe, respectively, which are very close to the values observed for the isomer shift (δ = 0.43 mm s^{-1}) and hyperfine magnetic splitting(519 kOe) obtained in this paper.

SEM micrograph of $LaFeO_3$ produced at 1100 °C (Fig. 4) shows coarse particles with non-uniform size and shape distribution.

Conclusion

The thermal decomposition of LaFe mixture in atmosphere of air to form $LaFeO_3$ involves the following pathways:

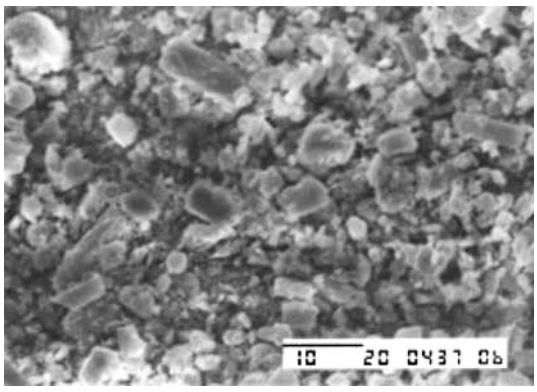

Fig. 4 Scanning electron micrograph showing the decomposition product of $La_2(C_2O_4)_3{\cdot}10H_2O$–$FeC_2O_4{\cdot}2H_2O$ (1:2 mole ratio) mixture calcined at 1100 °C for 2 h (scale bar 10 μm)

$$La_2(C_2O_4)_3{\cdot}10H_2O - 2FeC_2O_4{\cdot}2H_2O$$

$$\xrightarrow{182^\circ C} La_2(C_2O_4)_3 - 2FeC_2O_4$$

$$\xrightarrow{214^\circ C} La_2(C_2O_4)_3 - Fe_2O_3$$

$$\xrightarrow{376^\circ C} La_2O(CO_3)_2 - Fe_2O_3$$

$$\xrightarrow{440^\circ C} La_2O_2CO_3 - Fe_2O_3$$

$$\xrightarrow{660^\circ C} La_2O_3 - Fe_2O_3$$

$$\xrightarrow{1100^\circ C} LaFeO_3$$

Fe_2O_3 was detected as non-crystallite (amorphous) form at 250 °C and the crystallinity was improved by raising the calcination temperature up to 900 °C. XRD and Mössbauer techniques show the inability of orthoferrite formation before 1100 °C.

References

1. Goldman A (1993) Modern ferrite technology. Marcel Dekker, NY
2. Treves D (1965) Phys Rev 36:1033
3. Eibshutz M, Shtrikman S, Treves D (1967) Phys Rev 156:562
4. Coey JMD, Sawatzky GA, Morrish AH (1969) Phys Rev 184:334
5. Lukaszewicz JP (1991) Sens Actuators (B) 4:227
6. Obayashi H, Kudo T (1980) Nippon Kagaku Kaishi 1568
7. Aakawa T, Kurachi H, Shiokawa J (1985) J Mater Sci 4:1207
8. Li WB, Yoneyama H, Tamura H (1982) Nippon Kagaku Kaishi 761
9. Matsiwra Y, Matsushima S, Sakamato M, Sadaoka Y (1993) J Mater Chem 3:767
10. Kakihana M (1996) J Sol–Gel Sci Technol 6:7
11. Tascon J, Tejuca LG (1982) Z Phys Chem Neue Folge (Wiesbaden) 130:219
12. Falcon H, Goeta AE, Punte G, Carbonio RE (1997) J Sol State Chem 133:379
13. Popa M, Frantti J, Kakihana M (2002) Sol State Ionics 154–155:437
14. Suresh K, Panchapagesan TS, Patil KC (1999) Sol State Ionics 126:299
15. Zhang Q, Saito F (2001) J Mater Sci 36:2287
16. Sangaletti L, Depero LE, Allieri B, Nunziante P, Traversa E (2001) J Eur Ceram Soc 21:719
17. Vazquez C, Kagerler P, Lopez-Quintela MA, Sanches M, Rivas J (1998) J Mater Res 13:451
18. Balboul BAA, El-Roudi AM, Samir E-, Othman AG (2002) Thermochim Acta 387:109
19. Boyanov B, Khadzhiev D, Vasilev-Plavdiv V (1985) Thermochim Acta 93:89
20. Dollimore D (1987) Thermochim Acta 117:331
21. Diefallah EL-HM, Gabal MA, El-Bellihi AA, Eissa NA (2001) Thermochim Acta 376:43
22. Grosse G (1992) Mos-90, version 2.2. 2nd edn. Oskar-Maria-Graf-Ring, Munchen

23. Brady PR, Duncan JF (1964) J Chem Soc 653
24. Fluck E, Keler W, Nettwirth W (1963) Angew Chem 2:277
25. Diefallah EL-HM (1992) Thermochim Acta 202:1
26. Macklen ED (1968) J Inorg Nucl Chem 30:2689
27. Nakamura T, Shinjo T, Endoh Y, Yamamato N, Shiga M, Nakamura Y (1964) Phys Lett 12:178
28. Gabal MA, El-Bellihi AA, Ata-Allah SS (2003) J Mater Chem Phys 81:84
29. Kisner OC, Sunvar AW (1960) Phys Rev Lett 4:412
30. Music S, Ilkovac V, Ristic M (1992) J Mater Sci 27:1011
31. Jiangong L, Xiao Hong C, Anmin WT (1993) Phys Stat Sol (b) 176:177